Toward Compression-Field Analysis of Reinforced Concrete Solids

By F. J. Vecchio[1] and R. G. Selby[2]

Abstract: Finite-element formulations are presented for the analysis of reinforced concrete solids. Cracked reinforced concrete is treated as an orthotropic nonlinear elastic material based on a smeared, rotating crack model. Secant-stiffness moduli are defined for concrete and reinforcement, and these are used in the development of an eight-noded regular hexahedral element. Procedures are discussed by which the formulations can be implemented into existing linear elastic algorithms to provide nonlinear analysis capabilities. The constitutive relations implemented in the formulations are relations extrapolated from the two-dimensional models of the modified compression field theory (MCFT). The accuracy of the constitutive models and finite-element formulations are examined by analyzing a series of overreinforced beams subjected to bending and torsion. Excellent agreement is found between predicted and observed response. The performance characteristics and potential applications of the analysis procedure are discussed, and areas in need of further research are identified.

Introduction

Finite-element procedures for the three-dimensional analysis of reinforced concrete structures have been available for several years. The formulations that have been developed, often using different approaches, are typically quite sophisticated and powerful, and are constantly being improved. This advancement in technology, however, has not been matched by a similar effort to develop and implement realistic constitutive models to represent accurately the complex nonlinear behavior of cracked reinforced concrete. As such, the ability of finite-element procedures to model accurately reinforced concrete solids remains unsatisfactory (Collins et al. 1985).

The modified compression field theory (MCFT) (Vecchio and Collins 1986) was formulated to predict the response of reinforced concrete under general two-dimensional stress conditions. The theory treated cracked reinforced concrete as an orthotropic nonlinear elastic path-independent material based on a smeared, rotating crack model. Conditions of equilibrium and compatibility were treated in terms of average stresses and average strains. Local stress conditions at crack locations were also considered. Based on the results of an extensive series of panel tests, new constitutive relations were derived. Of particular significance were the effects of softening of concrete in compression due to co-acting transverse tensile strains, and the effects of postcracking tensile stresses in the concrete.

The constitutive relations of the MCFT were incorporated into various two-dimensional finite-element algorithms (Adeghe 1986; Stevens et al. 1987; Cook and Mitchell 1988). In particular, a simple secant-stiffness-based fi-

[1]Assoc. Prof., Dept. of Civ. Engrg., Univ. of Toronto, Toronto, Ontario, Canada, M5S 1A4.

[2]Doctoral Student, Dept. of Civ. Engrg., Univ. of Toronto, Toronto, Ontario, Canada M5S 1A4.

Note. Discussion open until November 1, 1991. To extend the closing date one month, a written request must be filed with the ASCE Manager of Journals. The manuscript for this paper was submitted for review and possible publication on June 20, 1990. This paper is part of the ***Journal of Structural Engineering***, Vol. 117, No. 6, June, 1991. ©ASCE, ISSN 0733-9445/91/0006-1740/$1.00 + $.15 per page. Paper No. 25900.

nite-element formulation was developed that was adaptable to existing linear elastic algorithms (Vecchio 1990). Comparisons with test results showed that these formulations, on the strength of the constitutive modeling, typically provided excellent predictions of the nonlinear response of membrane-type structures (Vecchio 1989).

In this paper, the secant-stiffness-based formulation of a nonlinear finite-element analysis algorithm is extended to the three-dimensional case. Extrapolations of the constitutive relations of the MCFT are made and implemented into the formulation. By comparing the predictions obtained for a series of test beams, it is shown that accurate modeling of reinforced concrete solids can be achieved.

Element Formulation

In developing the stiffness formulations for a finite element, a material stiffness matrix **D** is required to relate stresses $\{\mathbf{f}\}$ to strains $\{\boldsymbol{\epsilon}\}$, i.e.

$$\{\mathbf{f}\} = \mathbf{D}\{\boldsymbol{\epsilon}\} \quad (1)$$

where $\{\mathbf{f}\} = [f_x f_y f_z v_{xy} v_{yz} v_{xz}]$; and $\{\boldsymbol{\epsilon}\} = [\epsilon_x \epsilon_y \epsilon_z \gamma_{xy} \gamma_{yz} \gamma_{xz}]$. The stiffness matrix **D** must be modified, according to an appropriate set of constitutive laws, in order to capture the nonlinear behavior of reinforced concrete. The form of the matrix **D** will also depend on the type of nonlinear solution algorithm employed. The formulations that follow assume a secant-stiffness approach.

Prior to cracking, reinforced concrete can be considered a linear elastic isotropic material, with **D** defined accordingly. After cracking, however, the concrete and the reinforcement can be considered to contribute separately to the composite stiffness. Thus, for a concrete element reinforced in n directions

$$\mathbf{D} = \mathbf{D}_c + \sum_{i=1}^{n} \mathbf{D}_{si} \quad (2)$$

where $\mathbf{D}_c$ = stiffness derived from the concrete; and $\mathbf{D}_{si}$ = stiffness arising from the reinforcement in the ith direction. There can be any number of reinforcement components, oriented in any direction.

Cracked concrete can be modeled effectively as an orthotropic material with the principal stress axes corresponding to the directions of the principal average strains. In addition, Poisson's effect can be considered negligible after cracking. Thus, the concrete material stiffness matrix evaluated with respect to the principal axes system, $\mathbf{D}_c'$, is

$$\mathbf{D}_c' = \begin{bmatrix} \bar{E}_{c1} & 0 & 0 & 0 & 0 & 0 \\ 0 & \bar{E}_{c2} & 0 & 0 & 0 & 0 \\ 0 & 0 & \bar{E}_{c3} & 0 & 0 & 0 \\ 0 & 0 & 0 & \bar{G}_{c12} & 0 & 0 \\ 0 & 0 & 0 & 0 & \bar{G}_{c23} & 0 \\ 0 & 0 & 0 & 0 & 0 & \bar{G}_{c13} \end{bmatrix} \quad (3)$$

where $\bar{E}_{c1}$, $\bar{E}_{c2}$, $\bar{E}_{c3}$, $\bar{G}_{c12}$, $\bar{G}_{c23}$, and $\bar{G}_{c13}$ are secant moduli. The secant moduli are defined as follows:

$$\bar{E}_{c1} = \frac{f_{c1}}{\epsilon_{c1}} \quad (4)$$

$$\bar{E}_{c2} = \frac{f_{c2}}{\epsilon_{c2}} \quad (5)$$

$$\bar{E}_{c3} = \frac{f_{c3}}{\epsilon_{c3}} \quad (6)$$

$$\bar{G}_{c12} = \frac{\bar{E}_{c1}\bar{E}_{c2}}{\bar{E}_{c1} + \bar{E}_{c2}} \quad (7)$$

$$\bar{G}_{c23} = \frac{\bar{E}_{c2}\bar{E}_{c3}}{\bar{E}_{c2} + \bar{E}_{c3}} \quad (8)$$

$$\bar{G}_{c13} = \frac{\bar{E}_{c1}\bar{E}_{c3}}{\bar{E}_{c1} + \bar{E}_{c3}} \quad (9)$$

where ϵ_{c1}, ϵ_{c2}, ϵ_{c3} = principal concrete strains ($\epsilon_{c1} > \epsilon_{c2} > \epsilon_{c3}$); and f_{c1}, f_{c2}, f_{c3} = principal concrete stresses in the first, second, and third directions, respectively.

For each reinforcement component, a corresponding material stiffness matrix $\mathbf{D}'_{si}$ can be determined as

$$\mathbf{D}'_{si} = \begin{bmatrix} \rho_i \bar{E}_{si} & 0 & 0 & 0 & 0 & 0 \\ 0 & 0 & 0 & 0 & 0 & 0 \\ 0 & 0 & 0 & 0 & 0 & 0 \\ 0 & 0 & 0 & 0 & 0 & 0 \\ 0 & 0 & 0 & 0 & 0 & 0 \\ 0 & 0 & 0 & 0 & 0 & 0 \end{bmatrix} \quad (10)$$

where ρ_i = reinforcement ratio; and $\bar{E}_{si}$ = secant modulus. The modulus is calculated from

$$\bar{E}_{si} = \frac{f_{si}}{\epsilon_{si}} \quad (11)$$

where ϵ_{si} and f_{si} = average strain and average stress in the reinforcement, respectively.

Note that the material stiffnesses $\mathbf{D}'_c$ and $\mathbf{D}'_{si}$ are evaluated with respect to their principal (i.e. local) axes systems. Prior to their being added together according to (2), the component stiffnesses must be transformed to the global-axes system. The transformations required are as follows:

$$\mathbf{D}_c = \mathbf{T}_c^T \mathbf{D}'_c \mathbf{T}_c \quad (12)$$

and

$$\mathbf{D}_{si} = \mathbf{T}_{si}^T \mathbf{D}'_{si} \mathbf{T}_{si} \quad (13)$$

where the transformation matrix $\mathbf{T}$ is given (Cook 1981) by

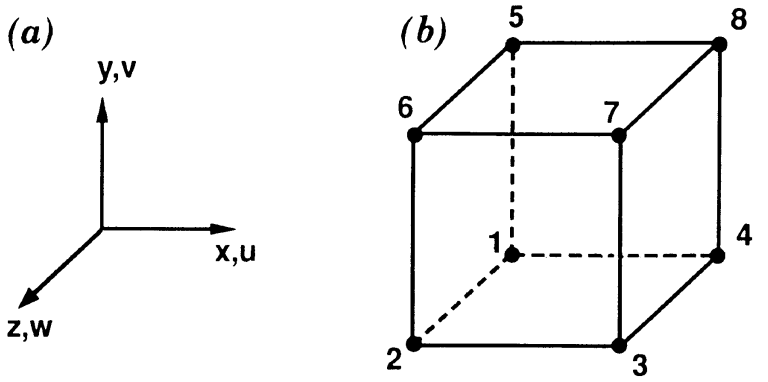

FIG. 1. Eight-Noded Regular Hexahedron Finite Element

$$\mathbf{T} = \begin{bmatrix} l_1^2 & m_1^2 & n_1^2 & l_1m_1 & m_1n_1 & n_1l_1 \\ l_2^2 & m_2^2 & n_2^2 & l_2m_2 & m_2n_2 & n_2l_2 \\ l_3^2 & m_3^2 & n_3^2 & l_3m_3 & m_3n_3 & n_3l_3 \\ 2l_1l_2 & 2m_1m_2 & 2n_1n_2 & l_1m_2 + l_2m_1 & m_1n_2 + m_2n_1 & n_1l_2 + n_2l_1 \\ 2l_2l_3 & 2m_2m_3 & 2n_2n_3 & l_2m_3 + l_3m_2 & m_2n_3 + m_3n_2 & n_2l_3 + n_3l_2 \\ 2l_3l_1 & 2m_3m_1 & 2n_3n_1 & l_3m_1 + l_1m_3 & m_3n_1 + m_1n_3 & n_3l_1 + n_1l_3 \end{bmatrix} \quad \ldots (14)$$

The direction cosines l, m, n define the direction of the principal concrete strains [in (12)] or that of the reinforcement component [in (13)]. The material stiffness matrix **D** that results will be fully populated and symmetric.

Having determined an appropriate material stiffness **D**, the element stiffness matrix **k** for a particular element can be evaluated using standard procedures [e.g. Cook (1981)]. As well, prestrain effects in the component materials (e.g. thermal expansion, prestressing in reinforcement, concrete shrinkage, residual strains from prior loading, etc.) can be rigorously accounted for in a manner previously described (Vecchio 1990).

An eight-noded regular hexahedron (see Fig. 1), based on linear displacement functions, was chosen for the finite-element formulation. Although it is a low-powered element, when used in sufficient quantity it can adequately represent the strain gradients assumed to occur in reinforced concrete. [Similar low-powered two-dimensional elements were found to accurately model the response of reinforced concrete membrane structures (Vecchio 1989).] The 24-degree-of-freedom hexahedral element allows explicit evaluation of the element stiffness matrix, avoiding costly numerical integration procedures. Higher-powered elements, if desired, can be formulated using the same material stiffness approach.

Constitutive Modeling

The secant-stiffness approach utilized in defining the material stiffness matrix is amenable to the implementation of a diverse variety of constitutive models. It is important to note that in the definition of the secant moduli, in (4)–(6), the use of uniaxial stress-strain relations is neither implied nor suggested. Multiaxial, inelastic, or hysteretic formulations resulting in strain shifts are easily accommodated by implementing the facility for material prestrains, as discussed. The finite-element formulation and analyses discussed

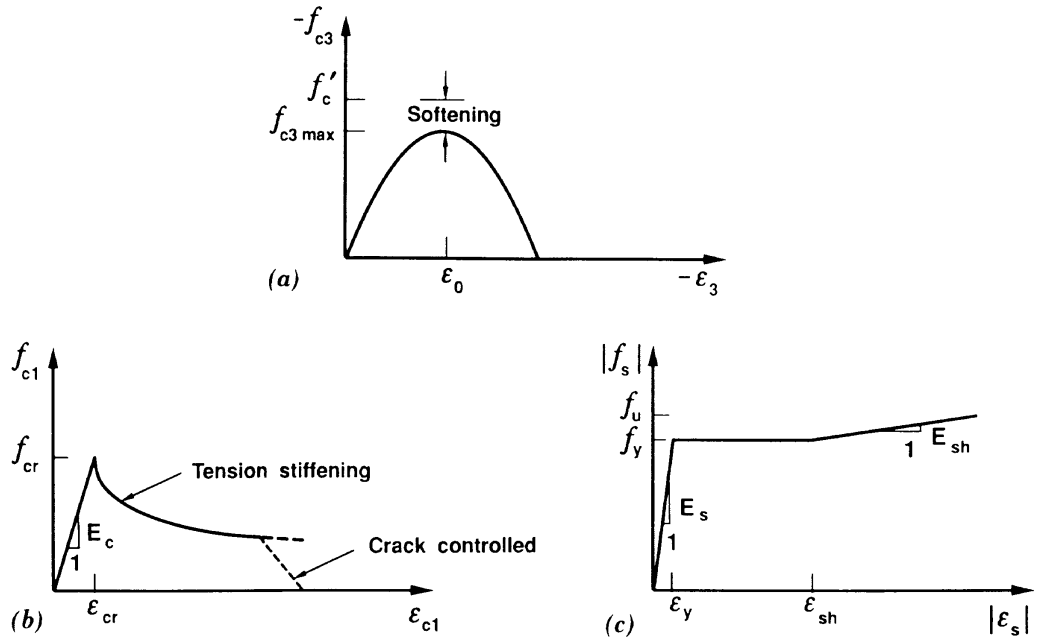

FIG. 2. MCFT Constitutive Relations: (*a*) Concrete in Compression; (*b*) Concrete in Tension; (*c*) Reinforcement

hereafter were based on an implementation of the constitutive models of the modified compression field theory (MCFT) (Vecchio and Collins 1986), extrapolated to three dimensions. The relations used are as follows.

For concrete in the direction of the largest principal compressive strain (ϵ_{c3}), the stress-strain relation used is

$$f_{c3} = f_{c3_{max}}\left[2\left(\frac{\epsilon_{c3}}{\epsilon_0}\right) - \left(\frac{\epsilon_{c3}}{\epsilon_0}\right)^2\right] \quad \ldots\ldots (15)$$

where

$$f_{c3_{max}} = \frac{f'_c}{0.8 - \left(0.34\,\frac{\epsilon_{c1}}{\epsilon_0}\right)} \quad \ldots\ldots (16)$$

and where f'_c = concrete cylinder strength; and ϵ_0 = cylinder strain at peak strength [see Fig. 2(*a*)]. (Note: both f'_c and ϵ_0 are negative quantities.) The reduction in the maximum attainable stress $f_{c3_{max}}$, as a function of the coexisting transverse tensil strain ϵ_{c1}, typically represents a significant softening effect.

For concrete in the direction of the principal tensile strain (ϵ_{c1}), prior to concrete cracking, a linear relation is used

$$f_{c1} = E_c\epsilon_{c1}, \qquad 0 < \epsilon_{c1} < \epsilon_{cr} \quad \ldots\ldots (17)$$

where E_c = initial tangent modulus

$$E_c = \frac{2f'_c}{\epsilon_0} \quad \ldots\ldots (18)$$

ϵ_{cr} = cracking strain

$$\epsilon_{cr} = \frac{f_{cr}}{E_c} \quad (19)$$

and f_{cr} = cracking stress

$$f_{cr} = 0.33\sqrt{f'_c} \text{ (MPa)} \quad (20)$$

After cracking, the decaying function

$$f_{c1} = \frac{f_{cr}}{1 + \sqrt{200\epsilon_{c1}}} \quad (21)$$

is used to reflect the tension-stiffening effects that are important in accurately predicting an element's load-deformation response [see Fig. 2(*b*)].

The average tensile stresses in the concrete must be transmitted across cracks. Thus, the stress f_{c1} must not be greater than the sum of the reverse of strength provided by the reinforcement crossing the crack. Algebraically

$$f_{c1} \leq \sum_{i=1}^{n} (\cos \theta_{ci})^2 \rho_i (f_{yi} - f_{si}) \quad (22)$$

where f_{yi} = yield stress of the reinforcement; f_{si} = average tensile stress in the reinforcement; and θ_{ci} = angle between the reinforcement and the normal to the crack surface. If the condition of (22) is not satisfied, then f_{c1} must be reduced accordingly.

Currently, in the absence of a complete three-dimensional model, the intermediate principal stress f_{c2} is evaluated using the same relationships. Thus, if ϵ_{c2} is compressive, then (15)–(16) are used substituting ϵ_{c2} for ϵ_{c3}; if ϵ_{c2} is tensile, then (17)–(21) are used.

Stresses in the reinforcement f_{si}, are evaluated according to a trilinear relation as follows:

$$f_{si} = E_{si}\epsilon_{si} \qquad \epsilon_{si} < \epsilon_{yi} \quad (23a)$$

$$f_{si} = f_{yi} \qquad \epsilon_{yi} < \epsilon_{si} < \epsilon_{shi} \quad (23b)$$

$$f_{si} = f_{yi} + E_{shi}(\epsilon_{si} - \epsilon_{shi}) < f_{ui} \qquad \epsilon_{si} > \epsilon_{shi} \quad (23c)$$

where f_{yi} = yield stress of the reinforcement; E_{si} = elastic modulus; E_{shi} = strain-hardening modulus; ϵ_{yi} = yield strain; and ϵ_{shi} = strain at the commencement of strain hardening [see Fig. 2(*c*)]. Perfect bond between the concrete and the reinforcement is assumed.

Analysis Procedure

A procedure for the nonlinear analysis of reinforced concrete solids was attained by incorporating the material and element formulations described earlier into an iterative linear elastic finite-element algorithm (program SPARCS, developed by the writers). A flowchart identifying the major steps in the analysis scheme is given in Fig. 3. In the iterative procedure, the

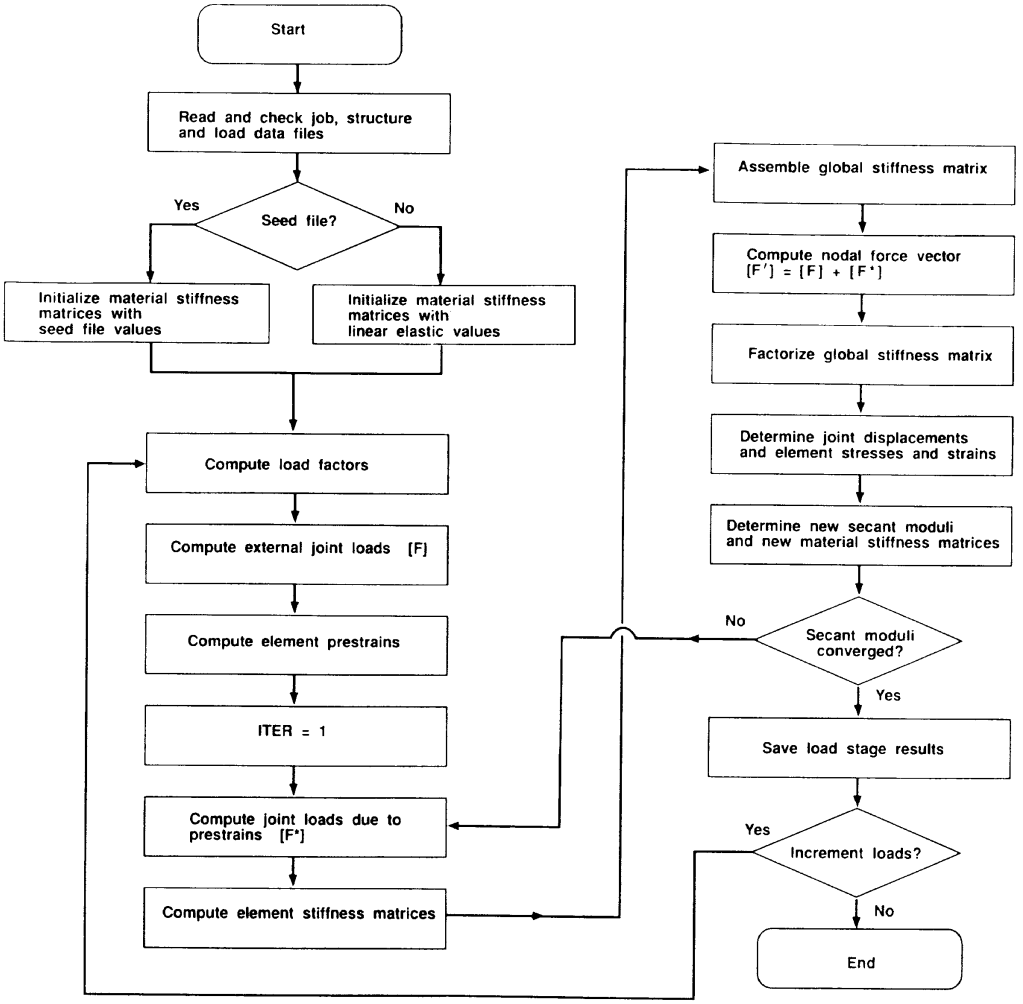

FIG. 3. Flowchart for Nonlinear Analysis Algorithm

material stiffness **D** and element stiffness **k** matrices for each element are progressively refined until convergence is achieved.

In initiating an analysis, an initial estimate of the material stiffness can be made by assuming linear elastic isotropic values. Alternatively, the stiffnesses determined in a previous analysis (e.g., in preceding load stage) can be used as the starting values. Given the material stiffnesses, the element and structure stiffness matrices are assembled. Cholesky decomposition is used to solve for the nodal displacements, from which element strains are calculated. The Jacobi method is then used to determine principal strains and corresponding directions. From the calculated strains, the corresponding stresses and secant moduli are determined, and new stiffness matrices are formed. If the secant moduli have changed, the structure is reanalyzed using the newly computed moduli and the procedure is repeated. Satisfactory convergence is usually achieved within 20–30 iterations. Note that if material prestrains are involved, the nodal-force vector must be recalculated through each iteration of the procedure.

SAMPLE CALCULATIONS

The analysis procedure described herein is simple and easily adaptable to

most existing linear elastic finite-element programs. The procedure is found to have good convergence characteristics and is numerically stable for a wide range of structural analysis conditions. Calculations derived from the following simple example will serve as an illustration.

Consider a single element subjected to a uniform three-dimensional stress condition. This could be interpreted as the stress condition at a point, in a larger structure, as determined from a global analysis of some kind. The properties of the element are $f'_c = -35$ MPa; $f_{cr} = 1.95$ MPa; $\epsilon_0 = -0.0025$; $E_c = 28{,}500$ MPa; $E_s = 200{,}000$ MPa; $f_y = 400$ MPa; $\rho_x = 0.035$; $\rho_y = 0.035$; and $\rho_z = 0.0008$. The element is assumed to be subjected to the following stress condition:

$$\{\mathbf{f}\} = [-6.0\ 1.0\ 0\ 4.0\ 3.0\ 3.0]\text{MPa} \quad \ldots\ldots\ldots\ldots\ldots\ldots\ldots\ldots\ldots\ldots\ldots\ldots \quad (24)$$

Note that the element is heavily reinforced in two directions, which is often the case in nuclear-containment and offshore structures. With such high re-

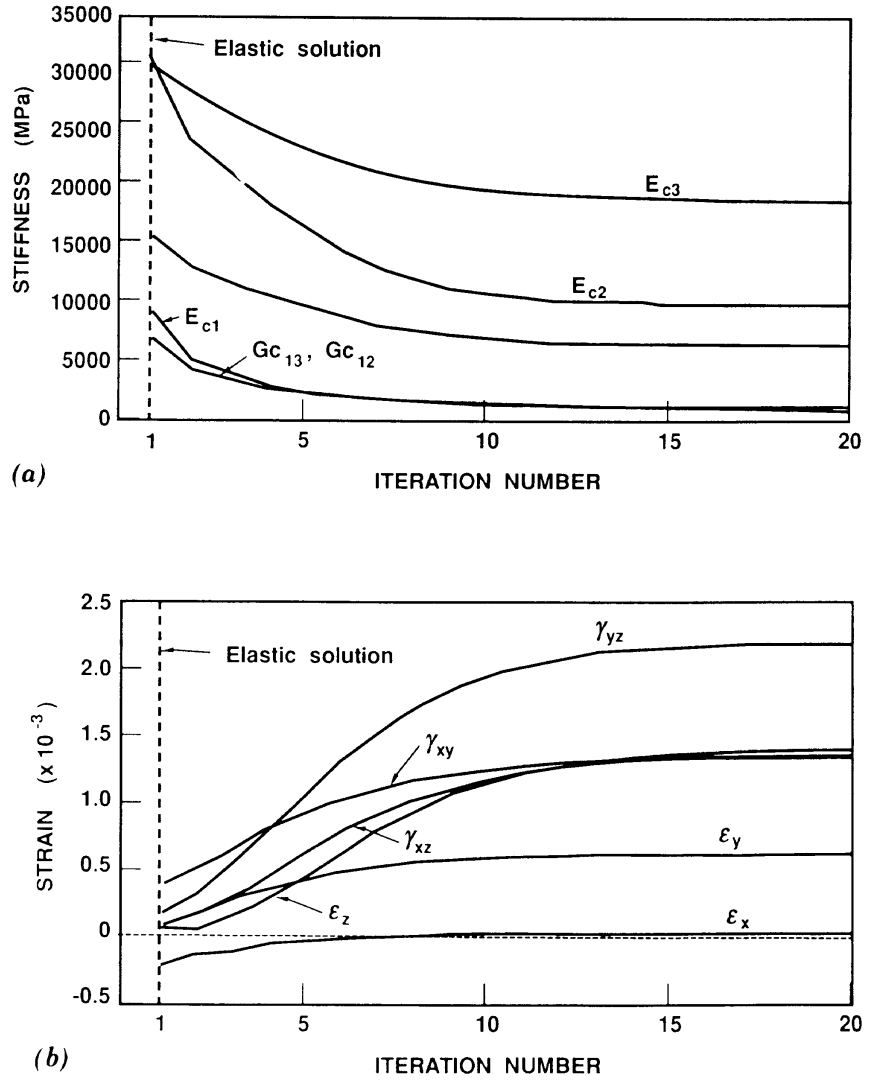

FIG. 4. Convergence Characteristics from Sample Analysis: (*a*) Secant Moduli; (*b*) Strains

inforcement ratios, realistic constitutive modeling is critical to the accurate prediction of structural response.

The response of the element was calculated using the program SPARCS, based on the forrmulations described. The analysis required 26 iterations to reach the convergence criteria specified. The first iteration assumed linear isotropic behavior in defining the material-stiffness matrix. Each successive iteration was based on the strains calculated in the previous cycle. The final strains corresponding to the given load condition were found to be

$$\{\epsilon\} = [-0.038\ 0.631\ 1.402\ 1.351\ 2.212\ 1.364] \times 10^{-3} \quad (25)$$

Shown in Fig. 4 are the convergence patterns exhibited by the secant moduli and by the element strains. The secant moduli are seen to initially undergo rapid change as behavior moves from uncracked isotropic to cracked orthotropic response. Thereafter, the secant moduli generally converge to stable values. The strain quantities are also seen to gradually converge, generally in a monotonic manner. It is anticipated that the number of cycles needed for satisfactory convergence could be reduced by implementing a variation of the Newton-Raphson technique or some other method.

In general, the procedure has been found to exhibit similar convergence and stability characteristics regardless of structure size (i.e. number of elements) or element properties (e.g. reinforcement patterns). Also, localized postultimate behavior is modeled without difficulty.

Corroboration with Test Data

To obtain a measure of the suitability and accuracy of the three-dimensional formulation, an investigation was undertaken to model the response of two series of beams tested in torsion (Onsongo 1978). The beams represented a difficult test of the analysis procedure because of the complex loading conditions, involving combined flexure and torsion, and because the beams were generally overreinforced and governed by failure of the concrete. The beams were heavily instrumented, providing many high-quality data against which the theoretical response would be compared.

The test program was comprised of two series of five beams each. The "torsion-bending-overreinforced" (TBO) series of beams were overreinforced, designed such that neither the longitudinal nor the transverse (i.e. hoop) reinforcement would yield. The "torsion-bending-underreinforced" (TBU) series of beams were underreinforced and designed such that at least some of the reinforcing steel would yield prior to failure. All the beams within a series had the same reinforcement arrangement and approximately the same concrete strength. The test variable was the ratio of moment to torque applied. The testing arrangement of specimens and cross-sectional details are given in Fig. 5; the loading conditions are defined in Table 1.

Since the beams were subjected to constant moment and torque along their length, only a partial length of the test beams was considered in the analysis. A 750 mm length was modeled using a mesh of 1,200 elements and 1,760 nodes (see Fig. 6, and Table 2), resulting in 5,280 degrees of freedom. Three elements were used through the thickness of the webs and flanges, and 10 layers of elements were used along the length. The bending moments

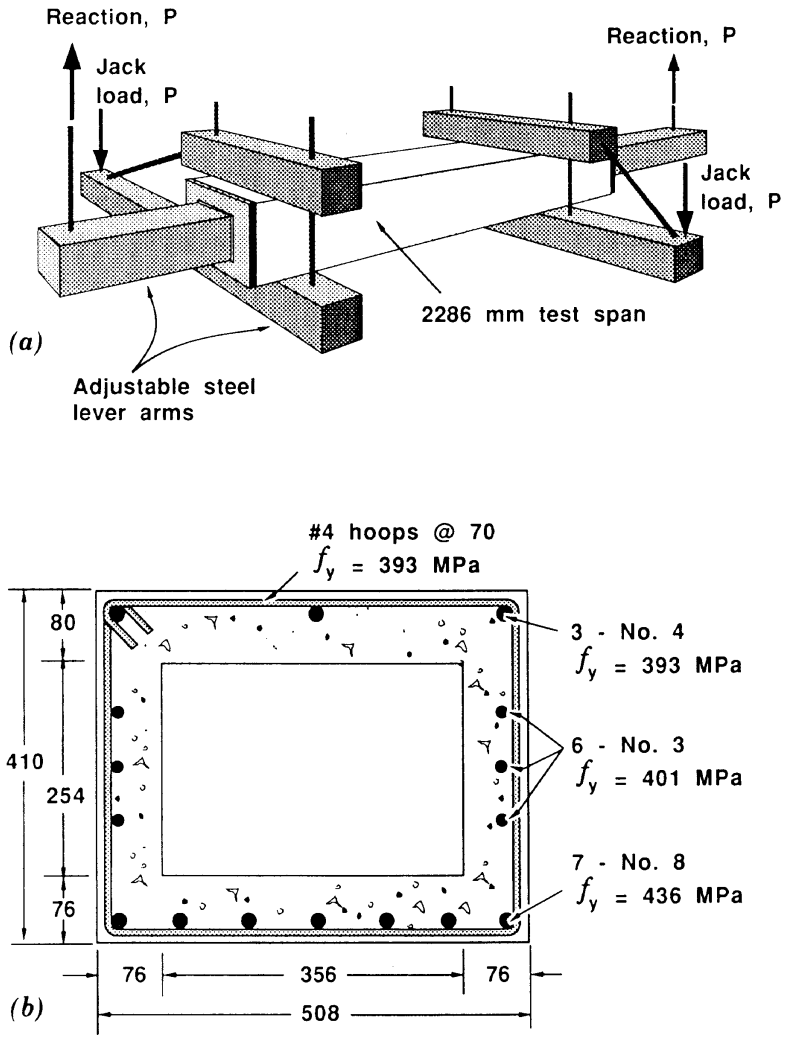

FIG. 5. Onsongo (1978) Test Beams: (*a*) Testing Arrangement; (*b*) Cross-Section Details

TABLE 1. Test Beam Parameters and Results

Beam (1)	f'_c (MPa) (2)	ϵ_0 (3)	T/M (4)	Experimental M_u (MPa) (5)	Experimental T_u (MPa) (6)	Experimental Failure mode (7)	Theoretical M_u (MPa) (8)	Theoretical T_u (MPa) (9)	Theoretical Failure mode (10)	Experimental/ theoretical (11)
TBO1	19.5	0.0024	0	401	0	CC-TF	365	0	CC-TF	1.099
TBO2	19.7	0.0024	0.261	334	78	CC-TF	313	72	CC-TF	1.067
TBO3	19.1	0.0024	0.701	232	143	CC	234	144	CC-AF	0.992
TBO4	20.4	0.0024	1.524	117	149	CC	120	155	CC-AF	0.972
TBO5	20.6	0.0024	5.059	35	143	CC; LT	35	148	CC-AF; LT	0.987
TBU1	34.8	0.0031	0	551	0	CC-TF; LB	525	0	CC-TF; LB	1.050
TBU2	34.8	0.0031	0.261	439	104	CC-TF; LB	466	122	CC-TF; LB	0.942
TBU3	34.8	0.0031	0.696	327	207	CC; LB, TB	331	210	CC-AF; LB, TB	0.988
TBU4	34.8	0.0031	1.509	147	195	CC; HAF	166	224	CC-AF; HT	0.866
TBU5	34.8	0.0031	5.059	41	175	CC; LT, HT	45	201	CC-AF; LT, HT	0.911

Note: CC = concrete crushing; TF = top face; AF = all faces of specimen; LT = yield of longitudinal steel in top face; LB = yield of longitudinal steel in bottom face; HT = yield of hoop steel in top face; and HAF = yield of hoops in all faces.

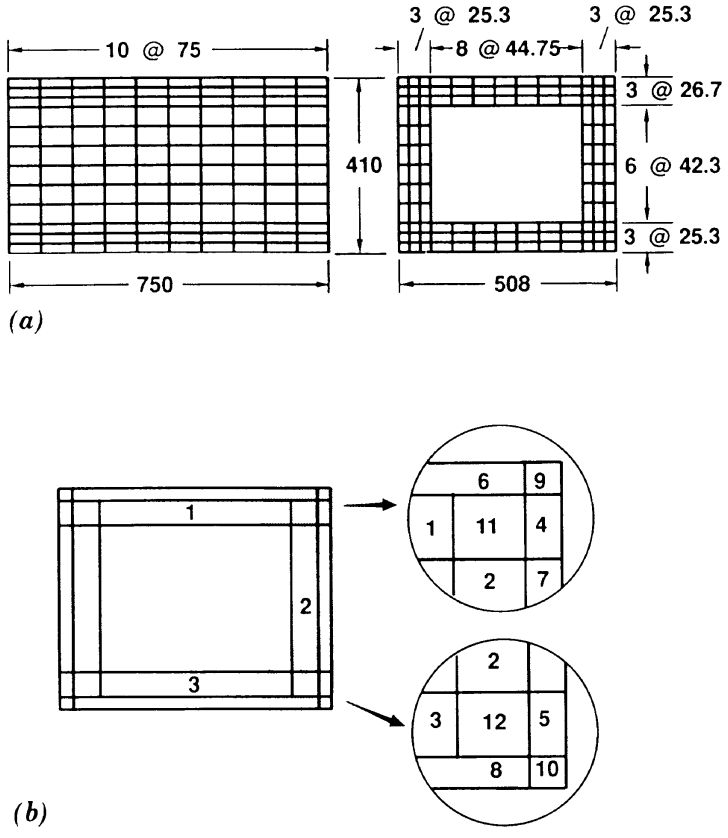

FIG. 6. Theoretical Modeling of Test Beams: (*a*) Finite-Element Mesh; (*b*) Reinforcement Details (See Also Table 2)

and torques were applied as nodal forces at the ends of the beams. The elements in the final layer at each end were assigned stiffer material properties to facilitate load transfer and preclude a premature end failure. The longitudinal reinforcement in the top and bottom flanges, and in the web, was uniformly smeared over the respective areas. The hoop reinforcement

TABLE 2. Modeling of Reinforcement

Material type number (1)	Reinforcement Ratio (%)		
	x (2)	y (3)	z (4)
1	1.076	0	0.949
2	0	1.112	1.104
3	1.112	0	9.247
4	0	4.473	0.949
5	0	4.473	9.247
6	4.303	0	0.949
7	0	4.473	1.104
8	4.473	0	9.247
9	4.303	4.473	0.949
10	4.473	4.473	9.247
11	1.076	1.112	0.949
12	1.112	1.112	9.247

was concentrated in the outermost band of elements, with two-thirds of the reinforcement being smeared in this zone. The remaining area of hoop reinforcement was smeared over the inner two bands of elements. Thus, the centroids of the smeared reinforcement essentially coincided with the locations of the actual reinforcement. The material strengths used were as determined from the test specimens.

The analyses were performed on a CRAY X-MP/24 supercomputer. The complete load-deformation response for each beam required approximately 80 min of central processing unit (CPU) time. The average number of iterations required per load stage was 10–15 at early load stages and 25–30 at later load stages. Approximately 23 seconds of CRAY CPU time was used per iteration.

The ultimate load and failure mode of the test beams were predicted very well. For the TBO series, the ratio of the experimental to theoretical ultimate strength had a mean of 1.02 and a coefficient of variation of 5.4%. For the TBU series, the mean and coefficient of variation were 0.96 and 6.8%, respectively. The results are summarized in Fig. 7 and Table 1. In the TBO series, the failure mode involved crushing of the concrete in the top flanges

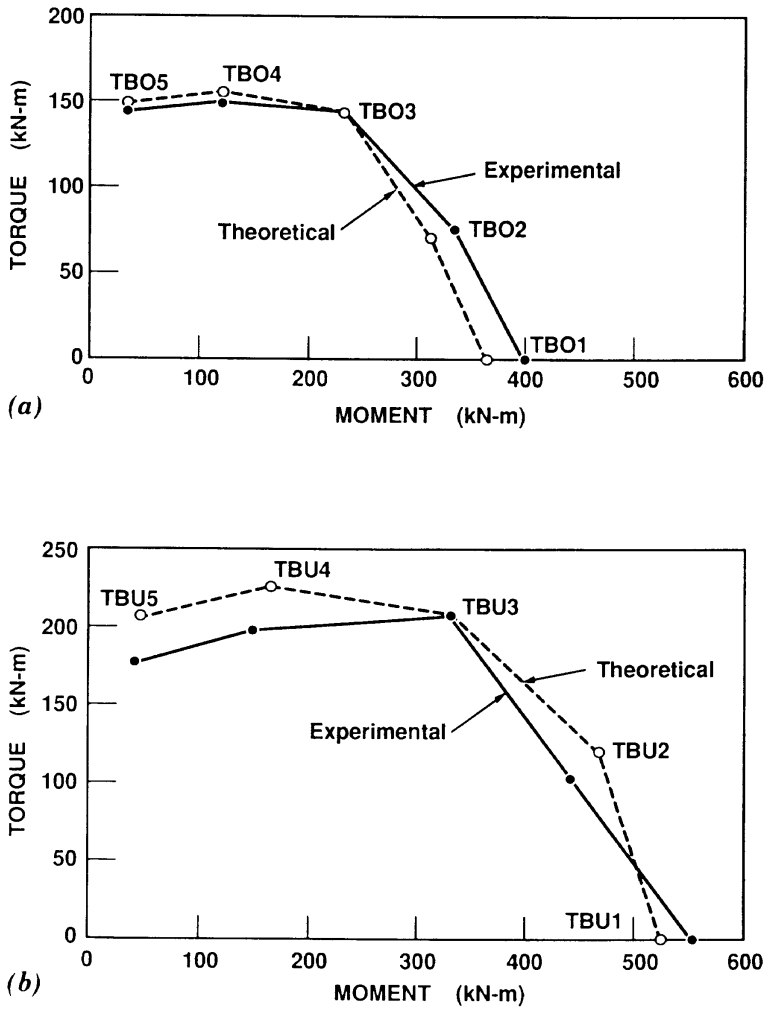

FIG. 7. Comparison of Experimental and Theoretical Ultimate Strengths: (*a*) TBO Series Beams; (*b*) TBU Series Beams

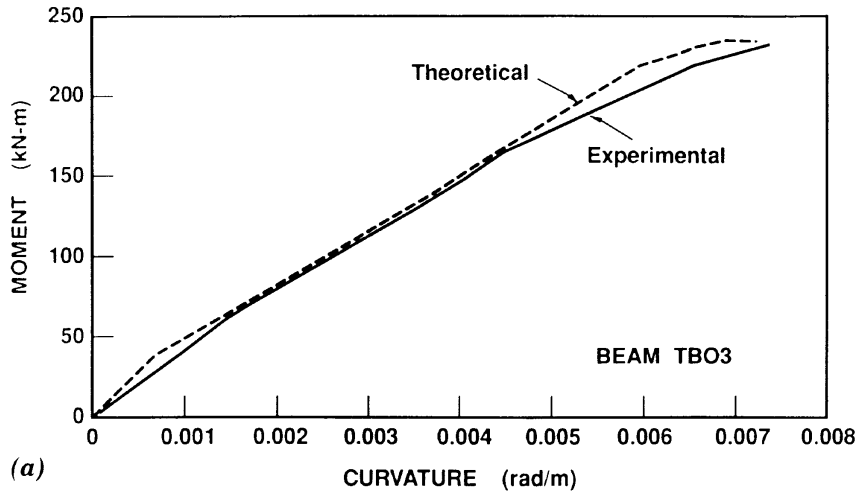

(a)

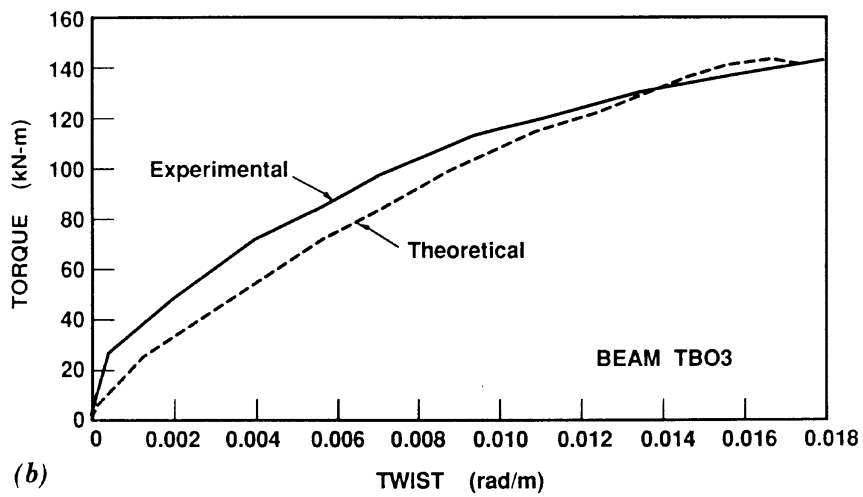

(b)

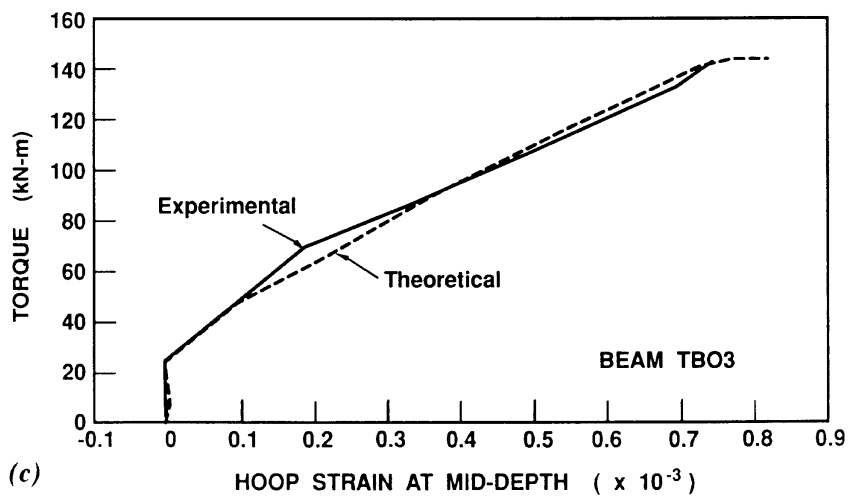

(c)

FIG. 8. Comparison of Experimental and Theoretical Response of Beam TBO3: (*a*) Moment-Curvature; (*b*) Torque-Twist; (*c*) Hoop Reinforcement Strains

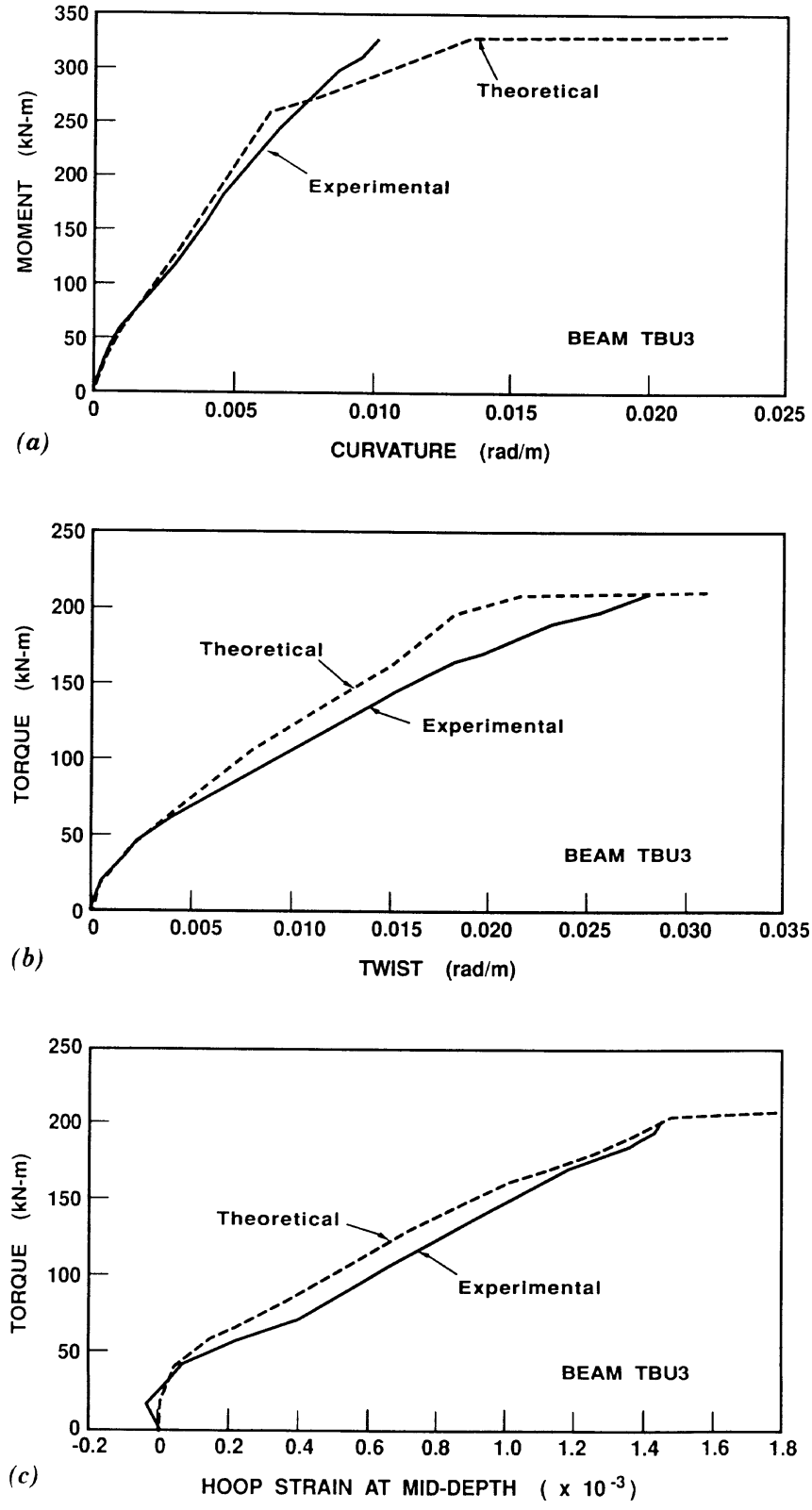

FIG. 9. Comparison of Experimental and Theoretical Response of Beam TBU3: (*a*) Moment-Curvature; (*b*) Torque-Twist; (*c*) Hoop Reinforcement Strains

for beams TBO1 and TBO2, shear/crushing of the concrete in the web and bottom flange for TBO3, shear/crushing of concrete on all four sides for TBO4, and shear/crushing in the webs and yielding of the longitudinal reinforcement in the top flange for TBO5. In all cases, these failure modes were accurately predicted by the analyses. Similar accuracy was achieved with the TBU series beams. It should be noted that difficulties in casting beams TBU2 and TBU4 resulted in premature failures, and thus lower than predicted strengths. In the theoretical analysis of beam TBO1, local crushing at the ends caused by load-transfer problems resulted in the somewhat low predicted strength.

The load-deformation responses and local strain conditions in the beams were also modeled extremely well. Shown in Figs. 8 and 9, as typical examples, are aspects of the predicted versus observed response for beams TBO3 and TBU3. (Moment-curvature responses were determined from the longitudinal strains at midspan; torque-twist curves were obtained by integrating the shear strains around the outer band of elements at midspan.) The predicted moment-curvature responses are seen to be in good agreement with the experimental values at all stages of loading [see Figs. 8(*a*) and 9(*a*)]. In the torque-twist behavior of beam TBO3 [Fig. 8(*b*)], the torsional stiffness is somewhat overestimated initially and underestimated in the late stages of loading, but is in generally good agreement. The reduced torsional rigidity observed near ultimate load is partially related to spalling of the concrete cover, which the theoretical analysis did not attempt to model. For beam TBU3, the torsional stiffness is initially slightly overestimated [see Fig. 9(*b*)]. Shown in Figs. 8(*c*) and 9(*c*) are the strains in the hoop reinforcement measured in the web at the mid-depth of the beam. Again, excellent agreement is observed. Similar accuracy was attained in modeling the response of the other beams.

The constitutive modeling of the concrete proved to be a significant factor in obtaining accurate predictions of response. In particular, the compression softening effect in the beams subjected to high torques (e.g. beams TBO3, TBO4, TBO5) had a major influence. In these beams, failure occurred by shear/crushing of the concrete struts at principal compressive stresses typically well below the cylinder strength. To have ignored the softening effect due to the large transverse tensile strains present would have resulted in highly overestimated ultimate strengths. To have ignored the postcracking tensile stresses in the concrete (i.e. tension stiffening effect) would have led to much larger estimated deformations in all beams.

Thus, strains, deformations, ultimate strengths, and failure modes were all modeled with good accuracy. The finite-element mesh used to model the beams, although somewhat coarse, appeared to adequately capture the complex nonlinear behavior of the beams. A finer mesh would no doubt have led to improved modeling. In particular, more elements through the wall thickness of the members would have allowed one to account for the effects of spalling as well as allowing for more accurate representation of the reinforcement details. However, given the current high computational demands of the procedure, an analysis using a finer discretization was not feasible.

Analysis Applications

Full three-dimensional nonlinear finite-element analysis of reinforced concrete structures remains a computationally intensive, time-consuming, and

expensive undertaking regardless of the formulation or constitutive models used. The formulation presented herein remains bound by these constraints, and thus its application potential is limited. However, the formulation's demonstrated ability to accurately model the complex nonlinear response of reinforced concrete solids does provide for some practical applications.

It is common procedure in the analysis of large or complex structures (e.g. offshore structures) to undertake a design check by first employing a linear elastic analysis to determine force distributions within the structures. From the forces determined, local stresses are then computed and checked for safety using some form of local nonlinear or limit-states approach. (The redistribution of forces caused by nonlinear behavior is generally not considered.) In this case, a local nonlinear analysis using the formulations presented (i.e. a one-element model) would give a realistic appraisal of local behavior such as reinforcement stresses, crack widths, deformations, and factor of safety. This could quickly and easily be performed on a personal computer.

The analysis procedure could also be a viable tool in the analysis and design of individual structural members of complex geometry or loading, or for which an accurate determination of strength or deformation response is required. The procedure can be useful in research applications to investigate, for example, the influences of stirrup spacing, cover, confinement, and other design variables.

With respect to global nonlinear analysis of complete structures, currently such an analysis would only be deemed viable and necessary under unusual conditions. However, with future improvements expected in computer technology and finite-element formulations, global nonlinear analysis may become more practical.

Needed Research

The constitutive relations currently used were extrapolated from a two-dimensional model derived from test data. Work is required to refine and verify the accuracy of the three-dimensional formulations. In particular, for concrete in the direction of the largest principal compressive strain (ϵ_{c3}), the pronounced softening effect is currently only dependent on the largest principal tensile strain (ϵ_{c1}). It would intuitively seem likely that the intermediate strain (ϵ_{c2}) should have some influence, and that this influence would differ depending on whether ϵ_{c2} was tensile or compressive. Similar questions exist regarding the relation for the principal tensile stress f_{c1}. Specifically, if concrete is also cracked in the intermediate principal strain direction (i.e., $\epsilon_{c2} > \epsilon_{cr}$), then a more rapidly decaying $f_{c1}:\epsilon_{c1}$ response would be expected. Stress-strain relations for the intermediate direction ($f_{c2}:\epsilon_{c2}$), both for tension and compression, are also in need of much further study. Finally, the current constitutive models do not allow for strength increases due to confinement, or strength decreases due to reversed or cyclic loading. These influences should also be addressed.

With respect to the finite-element formulation, work is required to make the algorithm more efficient. Significant improvements in efficiency could be attained by implementing a Newton-Raphson technique or equivalent to reduce the number of iterations required per load stage. In addition, the solver currently employed in SPARCS stores the stiffness matrix bandwidth in

core memory. By implementing a more efficient frontal solver and storing the stiffness matrix on disk, larger structures could be analyzed and computation time could be reduced. The analysis of beam members would be greatly simplified by applying constraint equations to eliminate degrees of freedom. Specifying nodes to deform in a controlled manner (e.g. plane sections remain plane, etc.) may erode accuracy somewhat but could reduce the computational requirements to where meaningful nonlinear three-dimensional analyses could be performed on a personal computer. Finally, development of higher-order elements and transition elements could facilitate, in some cases, more efficient modeling of structures.

Conclusions

A nonlinear finite-element program (SPARCS) was developed for the analysis of reinforced concrete solids. The program was based on an iterative secant stiffness formulation, and utilized a low-powered eight-noded brick element. The three-dimensional constitutive relations incorporated into the formulation were ones extrapolated from the two-dimensional relations defined in the modified compression field theory (MCFT). The adequacy of the constitutive models and finite-element formulations were examined by analyzing a series of overreinforced hollow beams subjected to combined bending and torsion.

The behavior of the test beams was accurately modeled by the theoretical analyses. Local strains, overall load-deformation response, ultimate strength, and failure modes were all predicted accurately. The indication was that the constitutive relations generalized from the MCFT provided a realistic description of complex nonlinear behavior in reinforced concrete solids. In particular, the effects of compression softening and tension stiffening, observed to be significant factors in the behavior of the test beams, were well represented.

The secant stiffness formulation developed resulted in a simple but effective means by which nonlinear finite-element analyses could be implemented. The stiffness formulations retained a form that provided much freedom in the type of constitutive relations that could be used, as well as being easily adaptable to most existing linear elastic finite-element programs. The analysis algorithm used demonstrated numerical stability and good convergence characteristics. The simple solid rectangular element formulated and utilized in the analyses was able to provide sufficient accuracy in modeling the test beams.

Additional research is needed to develop improved constitutive models, more efficient analysis algorithms, and more powerful elements. However, the tentative formulations presented herein demonstrated good potential ability to accurately model complex nonlinear behavior in reinforced concrete solids. Work will progress in this direction.

Acknowledgments

The work presented in this paper was made possible through funding from the Natural Sciences and Engineering Resarch Council of Canada. The authors wish to express their gratitude for the support received.

APPENDIX I. REFERENCES

Adeghe, L. N. (1986). "A finite element model for studying reinforced concrete detailing problems," thesis presented to the University of Toronto, at Toronto, Canada, in partial fulfillment of the requirements for the degree of Doctor of Philosophy.

Collins, M. P., Vecchio, F. J., and Mehlhorn, G. (1985). "An international competition to predict the response of reinforced concrete panels." *Canadian J. of Civ. Engrg.*, 12(3), 626–644.

Cook, R. D. (1981). *Finite element concepts and applications*, 2nd Ed., John Wiley and Sons, New York, N.Y.

Cook, W. D., and Mitchell, D. (1988). "Studies of disturbed regions near discontinuities in reinforced concrete members." *ACI Struct. J.*, 85(2), 206–216.

Onsongo, W. (1978). "The diagonal compression field theory for reinforced concrete beams subjected to combined torsion, flexure and axial load," thesis presented to the University of Toronto, at Toronto, Canada, in partial fulfillment of the requirements for the degree of Doctor of Philosophy.

Stevens, N. J., Uzumeri, S. M., and Collins, M. P. (1987). "Analytical modelling of reinforced concrete subjected to monotonic and reversed loading." *Publication Nov. 87-1*, Dept. of Civil Engineering, University of Toronto, Toronto, Canada.

Vecchio, F. J., and Collins, M. P. (1986). "The modified compression field theory for reinforced concrete elements subjected to shear." *J. Amer. Concrete Inst.*, 83(2), 219–231.

Vecchio, F. J. (1989). "Nonlinear finite element analysis of reinforced concrete membranes." *Amer. Concrete Inst. Struct. J.*, 86(1), 26–35.

Vecchio, F. J. (1990). "Reinforced concrete membrane element formulations." *J. of Struct. Engrg.*, ASCE, 116(3), 730–750.

APPENDIX II. NOTATION

The following symbols are used in this paper:

$\mathbf{D}$ = composite material stiffness matrix;
$\mathbf{D}_c$ = concrete material stiffness matrix;
$\mathbf{D}_s$ = reinforcement material stiffness matrix;
E_c = modulus of elasticity of concrete (initial tangent stiffness);
$\bar{E}_{c1}$ = secant modulus of concrete in principal tensile strain direction;
$\bar{E}_{c2}$ = secant modulus of concrete in intermediate principal strain direction;
$\bar{E}_{c3}$ = secant modulus of concrete in principal compressive strain direction;
E_{si} = modulus of elasticity of reinforcement in i-direction;
$\bar{E}_{si}$ = secant modulus of reinforcement in i-direction;
f'_c = compressive strength of concrete cylinder;
f_{c1} = principal tensile stress in concrete;
f_{c2} = intermediate principal stress in concrete;
f_{c3} = principal compressive stress in concrete;
f_{cr} = concrete cracking stress;
f_{si} = average stress in i-direction reinforcement;
f_x = element stress in x-direction;
f_y = element stress in y-direction;
f_{yi} = yield stress of i-direction reinforcement;
f_z = element stress in z-direction;
$\{\mathbf{f}\}$ = element stress matrix;
$\bar{G}_{c12}$ = secant shear modulus of concrete relative to 1,2-axes;

$\bar{G}_{c23}$ = secant shear modulus of concrete relative to 2,3-axes;
$\bar{G}_{c13}$ = secant shear modulus of concrete relative to 1,3-axes;
$\mathbf{k}$ = element stiffness matrix;
l = direction cosine with respect to x-axis;
m = direction cosine with respect to y-axis;
n = direction cosine with respect to z-axis;
$\mathbf{T}$ = transformation matrix;
v_{xy} = element shear stress relative to x,y-axes;
v_{yz} = element shear stress relative to y,z-axes;
v_{xz} = element shear stress relative to x,z-axes;
γ_{xy} = shear strain relative to x,y-axes;
γ_{yz} = shear strain relative to y,z-axes;
γ_{xz} = shear strain relative x,z-axes;
$\{\epsilon\}$ = element strain matrix;
ϵ_{c1} = principal tensile strain in concrete;
ϵ_{c2} = intermediate principal strain in concrete;
ϵ_{c3} = principal compressive strain in concrete;
ϵ_{cr} = strain in concrete at cracking;
ϵ_x = strain in x-direction;
ϵ_y = strain in y-direction;
ϵ_z = strain in z-direction;
ϵ_0 = strain in concrete cylinder at peak stress f'_c;
θ_{ci} = angle between i-direction reinforcement and normal-to-crack surface; and
ρ_i = steel reinforcement ratio in i-direction.